Earth and Space Science

RESEARCH ARTICLE
10.1029/2021EA001893

High-Resolution Climate Projections Over Minnesota for the 21st Century

Stefan Liess[1], Tracy E. Twine[1], Peter K. Snyder[1], William D. Hutchison[2], Gabriel Konar-Steenberg[1], Bonnie L. Keeler[3], and Kate A. Brauman[4,5]

[1]Department of Soil, Water, and Climate, University of Minnesota, St. Paul, MN, USA, [2]Department of Entomology, University of Minnesota, St. Paul, MN, USA, [3]Humphrey School of Public Affairs, University of Minnesota, St. Paul, MN, USA, [4]Institute on the Environment, University of Minnesota, St. Paul, MN, USA, [5]Global Water Security Center, The University of Alabama, Tuscaloosa, AL, USA

Key Points:

- Over northern and central Minnesota, winters and summers may be up to 6 and 4°C warmer, respectively, at the end of the 21st century
- Spring precipitation may increase by more than 1 mm per day over northern Minnesota
- Snow depth may decrease by more than 12 cm. Number of snow days per year may decrease by up to 55

Supporting Information:

Supporting Information may be found in the online version of this article.

Correspondence to:

S. Liess,
liess@umn.edu

Citation:

Liess, S., Twine, T. E., Snyder, P. K., Hutchison, W. D., Konar-Steenberg, G., Keeler, B. L., & Brauman, K. A. (2022). High-resolution climate projections over Minnesota for the 21st century. *Earth and Space Science*, *9*, e2021EA001893. https://doi.org/10.1029/2021EA001893

Received 25 JUN 2021
Accepted 2 FEB 2022

Author Contributions:

Conceptualization: Stefan Liess, Tracy E. Twine, Peter K. Snyder
Data curation: Stefan Liess, Gabriel Konar-Steenberg
Formal analysis: Stefan Liess, Tracy E. Twine, Gabriel Konar-Steenberg
Funding acquisition: Tracy E. Twine, Peter K. Snyder, William D. Hutchison, Bonnie L. Keeler, Kate A. Brauman
Investigation: Stefan Liess, Tracy E. Twine, Peter K. Snyder, Gabriel Konar-Steenberg

Abstract Minnesota is the state with the strongest winter warming in the contiguous United States. We performed regional climate projections at 10 km horizontal resolution using the Weather Research Forecasting model forced with eight CMIP5 GCMs. The selected GCMs have previously been found to be in relatively good agreement with observations over Minnesota compared to other members of the CMIP5 model ensemble. Our projections suggest ongoing warming in all seasons, especially in winter, as well as shallower snow depth and fewer days with snow cover. We expect significant increases in spring and early summer heavy precipitation events. Our comparisons between different time slices and two different emission scenarios indicate a climate for the state of Minnesota near the end of the 21st century that is significantly different from what has been observed by the end of the 20th century. Winters and summers are expected to be up to 6 and 4°C warmer, respectively, over northern and central Minnesota, and spring precipitation may increase by more than 1 mm d^{-1} over northern Minnesota. Especially over the central part of the state, winter snow depth is projected to decrease by more than 12 cm, and the number of days per year with snow depth of more than 2.54 cm (one inch) is expected to decrease by up to 55.

Plain Language Summary Minnesota is the state with the strongest winter warming in the contiguous United States. We performed regional projections of the climate across Minnesota for the middle and end of the 21st century. We selected the results from eight recent global climate model projections to calculate climate data over an area of 10 km by 10 km with a regional climate model. Our results indicate that the future climate for the state of Minnesota is likely to be significantly different from what has been observed near the end of the 20th century. Over northern and central Minnesota, winters and summers are expected to be up to 6 and 4°C warmer, respectively, near the end of the 21st century. Spring precipitation may increase by more than 1 mm d^{-1} over northern Minnesota. Over the central part of the state, winter snow depth is suggested to decrease by more than 12 cm. The number of days per year with snow depth of more than 2.54 cm (one inch) is expected to decrease by up to 55. These results are expected to influence regional decision-making related to agriculture, infrastructure, water resources, and other sectors.

1. Introduction

For almost a century, surface warming has had its largest amplitude in the higher latitudes of the Northern Hemisphere (Callendar, 1938). Over the last several decades, the Arctic region has warmed between 0.14°C per decade (Bekryaev et al., 2010) and 0.17°C per decade (Polyakov et al., 2002), which is more than twice the rate of the rest of the planet. With anthropogenic climate change, it may warm an additional 4–8°C by the end of this century (Harvey et al., 2015; IPCC, 2013, 2021). The U.S. state of Minnesota is strongly affected by this Arctic warming, particularly during winter, when the influence of Arctic air is most dominant (Wang et al., 2017) and when reductions in snow cover lower the surface albedo (Shi et al., 2013). Minnesota's winter warming is the strongest among the 48 contiguous United States (NCEI, 2021). Future projections indicate ongoing warming as well as significant increases in spring and early summer heavy precipitation events over the north central United States by the end of this century (Harding & Snyder, 2014).

Despite the clear signals of increased temperature and precipitation in models of future climate, the large-scale outputs of general circulation models (GCM) are difficult to integrate into regional, state, and local planning

Methodology: Stefan Liess, Tracy E. Twine, Peter K. Snyder, William D. Hutchison, Bonnie L. Keeler
Project Administration: Tracy E. Twine, Peter K. Snyder, William D. Hutchison, Bonnie L. Keeler
Resources: Stefan Liess, Tracy E. Twine, Peter K. Snyder, William D. Hutchison, Bonnie L. Keeler, Kate A. Brauman
Software: Stefan Liess, Tracy E. Twine, Peter K. Snyder, Gabriel Konar-Steenberg
Supervision: Tracy E. Twine, Peter K. Snyder, William D. Hutchison, Bonnie L. Keeler
Validation: Stefan Liess, Tracy E. Twine, Gabriel Konar-Steenberg
Visualization: Stefan Liess, Gabriel Konar-Steenberg
Writing – original draft: Stefan Liess
Writing – review & editing: Stefan Liess, Tracy E. Twine, Peter K. Snyder, Gabriel Konar-Steenberg, Kate A. Brauman

where climate information is required by decision makers over smaller areas, such as individual watersheds and counties. GCMs typically have resolutions coarser than 100 km, which is insufficient for these applications (Boé et al., 2007; Zorita & von Storch, 1999). Differentiating the impacts of climate change at finer spatial scales is particularly important and challenging in Minnesota, where many days of snow cover and many small-scale open water sources, such as lakes and rivers all contribute to variations on the ground that are typically not addressed by GCMs. In order to provide reasonable climate projections over Minnesota on the regional scale, we dynamically downscaled GCM projections from an eight-model ensemble to a higher spatial resolution (~10 km) by nesting a finer scale regional climate model (RCM).

An early review of dynamical downscaling efforts (Giorgi & Mearns, 1991) describes simulations as high as 0.5° x 0.5° horizontal resolution, which has later been improved to a range of 25–50 km in the comprehensive Coordinated Regional Downscaling Experiment (CORDEX; Giorgi et al., 2015), especially the North American branch (NA-CORDEX; McGinnis & Mearns, 2021), which is preceded by the North American Regional Climate Change Assessment Program (NARCCAP; Mearns et al., 2009). However, these simulations have an insufficient horizontal resolution to resolve the small-scale open water sources in Minnesota.

Other high-resolution studies like Liu et al. (2017) at a 4-km horizontal resolution typically do not provide a multimodel ensemble to address the uncertainty in future climate projections. Ensemble downscaling simulations are considered crucial for providing a better estimate of future climate change and an uncertainty range (Xu et al., 2018). The downscaling experiment by Ashfaq et al. (2016) is probably closest to the present study. It uses 11 GCMs, including seven of the eight in the present study, for dynamical downscaling over the contiguous United States at an 18-km horizontal resolution, but only addresses one midcentury RCP8.5 scenario.

2. Methods

We use a dynamical downscaling approach based on nesting GCM input data with the Weather Research and Forecasting (WRF) RCM (Skamarock et al., 2008) coupled to the Community Land Model (CLM; Dai et al., 2003) with a dynamic crop module. This model version, also known as WRF-CLM4crop, has previously been described by Harding et al. (2016) and Lu et al. (2015). Vegetation, soil, and other land surface parameters for WRF-CLM-4crop are taken from the annual cycle of the Moderate-resolution Imaging Spectroradiometer (MODIS) satellite product at a 30-s horizontal resolution (Zhang et al., 2006) and kept consistent between all simulations. Atmospheric boundary conditions include 6-hourly prognostic variables such as temperature, wind speed and direction, specific humidity, and geopotential height from the Coupled Model Intercomparison Project 5 (CMIP5) GCM archive (Taylor et al., 2012) at the Earth System Grid (Williams et al., 2009).

From more than 40 available GCMs, we selected eight that provide all necessary prognostic variables and show reliable large-scale results over the Midwestern United States (Table 1; Harding et al., 2013). We adjusted the model selection in Table 4 of Harding et al. (2013) to only include GCMs that produce reasonable downscaling results during all four seasons, since Harding et al. (2013) only studied the summer season. Therefore, we needed to exclude MIROC4h and the ACCESS models after a short test simulation with our WRF downscaling setup. CCSM4 is not listed in Table 4 of Harding et al. (2013) because 6-hourly input data were not available at that time. However, it is ranked highly in their Figure 5, so we included it in this study.

Our downscaling approach is based on one-way nesting between the global and regional domains and two-way nesting between the two regional domains, so our RCM results cannot modify the global domain. Our regional domains comprise an outer nest over a large portion of North America at a 50-km grid-cell horizontal resolution and an inner nest over Minnesota and adjacent areas at a 10-km grid-cell horizontal resolution (Figure 1). These two nests are connected via two-way nesting and thus influence one another. The southern end of the outer nest is extended to the Gulf of Mexico in order to capture the Great Plains Low Level Jet (GPLLJ), which transports much-needed moisture from the Gulf of Mexico into the Central United States, especially during the warmer seasons (Zhou et al., 2021). However, the extent in other directions is limited by available computing resources, and therefore other storms such as those that develop in the lee of the Rocky Mountains may be represented only by the GCM input data instead of the regional WRF simulations. The inner nest in Figure 1 includes all lake points as represented in our WRF version.

Table 1
List of GCMs for Boundary Conditions

Model	Institution	Resolution [°]	Reference
bcc-csm1-1	BCC (China)	1 x 1.33	(Wu et al., 2010)
CCSM4	NCAR (USA)	0.9 x 1.25	(Gent et al., 2011)
CMCC-CM	CMCC (Italy)	0.75 x 0.75	(Scoccimarro et al., 2011)
CNRM-CM5	CNRM-CERFACS (France)	1.5 x 1.5	(Voldoire et al., 2012)
GFDL-ESM2M	NOAA-GFDL (USA)	2 x 2.5	(Dunne et al., 2012)
IPSL-CM5A-LR	IPSL (France)	1.875 x 3.75	(Dufresne & Bony, 2008)
MIROC5	MIROC (Japan)	2.8 x 2.8	(Watanabe et al., 2010)
MRI-CGCM3	MRI (Japan)	1.125 x 1.125	(Yukimoto et al., 2012)

We compute downscaled regional climate projections for the historical period of 1980–1999; from the RCP4.5 scenario, which assumes a moderate amount of mitigation of GHG emissions (van Vuuren et al., 2011) for two 20-year periods of the 21st century (2040–2059 and 2080–2099); and from the RCP8.5 scenario, which assumes only a minimum of mitigation, for the 2080–2099 period (Riahi et al., 2011). For the state of Minnesota and surrounding regions, we use WRF to generate hourly averages of the following surface variables: 2-m air temperature, 2-m humidity, 10-m wind speed and direction, precipitation, downward solar radiation, net radiation, latent, sensible, and ground heat fluxes, snow depth, and soil temperature and moisture content at 10 layers to a depth of 2.5 m. The seasonal cycle of these values, especially precipitation, is generally improved by physical downscaling (Mendez et al., 2020).

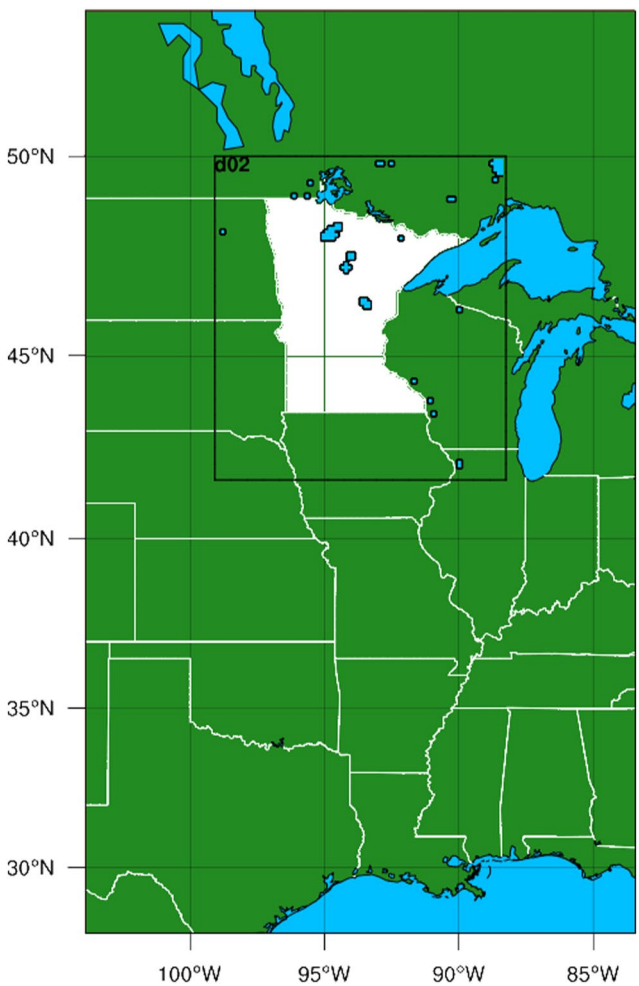

Figure 1. The outer (complete map) and inner grid (black frame) used for climate projections. The state of Minnesota is marked in white.

We perform a simple linear-scaling bias-adjustment (Teutschbein & Seibert, 2012) to surface air temperature and precipitation as described in equations 1–4 in Shrestha et al. (2017) using monthly mean observations as reported by the PRISM group (Daly et al., 2017). For snow depth, we perform bias adjustment with the NSIDC analysis that uses a combination of observed snow depth observations and the PRISM data set (Broxton et al., 2019; Zeng et al., 2018).

For the bias adjustment, we compare observations and WRF-simulated values from runs forced with each GCM for each monthly average (i.e., the average temperature difference over every January from 1980 to 1999 is calculated to receive one offset value for January at each grid point). Precipitation and snow depth are scaled by dividing monthly observational averages for 1981–2000 by monthly model values. The 2-m air temperature, precipitation, and snow depth error adjustments are then applied to data from each WRF run for each future scenario. Bias adjustment based on linear scaling retains the interannual variability but forces each multiyear monthly average for each GCM-forced WRF run in the historical simulations to equal the PRISM observations and NSIDC analysis, respectively. Linear scaling assumes that this offset carries through to the climate simulations of the future, so the simulations will now diverge in their calculations of these variables. Variables other than air temperature, precipitation, and snow depth are not adjusted because of lack of available observations. The prognostic variables for CCSM4 and CMCC-CM were previously bias-adjusted, so their historical multiyear monthly means match reanalysis data as described in Bruyère et al. (2014). We apply the same bias adjustment to the prognostic variables of all future scenarios for these two models.

In addition to analyzing WRF results forced from each GCM, we analyze the multimodel ensemble (MME) of each variable averaged over all WRF-driven

runs from all GCMs. Individual years of the simulations are treated as individual ensemble members in our analyses, and we adjusted the degrees of freedom in our statistical tests to account for lag-1 autocorrelation in our data, according to Wilks (2011), which allows a robust statistical analysis with 160 ensemble members per scenario. The advantage of this approach is that the variability of individual GCM simulations is being preserved, compared to smaller ensemble sizes with average GCM forcings. Although an MME approach with eight downscaled models should be considered as more reliable than individual model results, as previously demonstrated by Pincus et al. (2008), we also quantify bias adjustments for individual realizations of the historical climate in the next section.

3. Results and Discussion

3.1. Statewide Area Averages

The statewide area averages are computed by averaging over all grid cells with more than 50% of their area inside the state. Figure 2 depicts the statewide area averages for the bias adjustment offset for 2-m temperature and the adjustment factor for precipitation. These adjustments are applied to the WRF simulations to generate the bias-adjusted results. Although the GCM input data (Figures 2a and 2c) are closer to the observations, the WRF simulations (Figures 2b and 2d) convey the larger climate variability on the regional scale. However, the larger bias in the simulated precipitation is partly due to the choice of the 10-km horizontal resolution, which is within the 5–10 km range where neither convective parameterization nor a fully explicit approach provide convincing results (Molinari & Dudek, 1992). WRF-CLM4crop uses a convective parameterization scheme that adds subgrid-scale precipitation to the explicit approach and thus leads to an overestimation of precipitation in our results, in contrast to the study by Ashfaq et al. (2016), which uses cumulus convection parameterization on the larger 18 km grid or the study by Liu et al. (2017), which does not add cumulus convection parameterization to the smaller 4 km grid.

Although the trend analysis in the present paper is independent of linear scaling, we find that the analysis of absolute values and threshold values, such as the number of days per year with snow depth of more than a certain value benefits from the bias adjustment. It should also be noted that the downscaled results (Figures 2b and 2d) do not reflect the performance of individual GCMs (Figures 2a and 2c), they are merely a reflection of how WRF interprets the given sets of input data. Thus, although we use the term MME, our results are obtained with a single regional model at a single horizontal resolution, which makes the statistical analysis more feasible.

Many characteristics of individual GCM input data are also reflected in the WRF simulations during our 20-year historical simulation. For example, GFDL-ESM2M, IPSL-CM5A-LR, MIROC5, and MRI-CGCM3 have a warm bias in winter, whereas bcc-csm1-1 and CCSM4 have a cold bias in winter. CNRM-CM5 shows a slight warm bias from July to September, and MIROC5 depicts a strong warm bias from June to the end of the year. All WRF simulations apart from the ones driven by CMCC-CM have a cold bias in April and May, potentially due to the positive precipitation bias during this wet season. All area-averaged GCM input data are too dry in winter but only WRF runs driven by CMCC-CM, GFDL-ESM2M, IPSL-CM5A-LR, and MRI-CGCM3 share this GCM dry bias in winter. Especially in summer, all WRF runs are too wet based on the overrepresentation of convective precipitation, as discussed above (Figures 2c and 2d).

A detailed spatial analysis of the differences between the nonbias-adjusted WRF runs and the GCM input data in terms of comparability to observations is given in Figures S1 and S2 in the supplemental material. Figure S1 in Supporting Information S1 shows that historical 2-m temperatures in WRF are slightly too high in winter and too low in the spring rainy season compared with observation and also with GCM input. However, in summer, WRF simulations fit better with observations than the GCM input. Summer temperatures in the GCM input data are generally too high, but therefore match over the urban heat island of the Twin Cities metro area in southeast Minnesota, although urban climate is typically not included in GCMs. Fall temperatures are generally well represented in WRF and the GCM input data. Figure S2 in Supporting Information S1 depicts the general wet bias in the WRF MME that outweighs the aforementioned dry bias in some WRF simulations in winter. Although the relative precipitation bias is strongest in the dry summer season (Figure 2d), the absolute differences to observations are still not statistically significant over the southcentral region.

Figures S3–S6 in Supporting Information S1 compare future projections from the MMEs for GCMs and the WRF runs. Despite the wet bias in the WRF MME, they have similar trends for all three emission scenarios. Figure S7

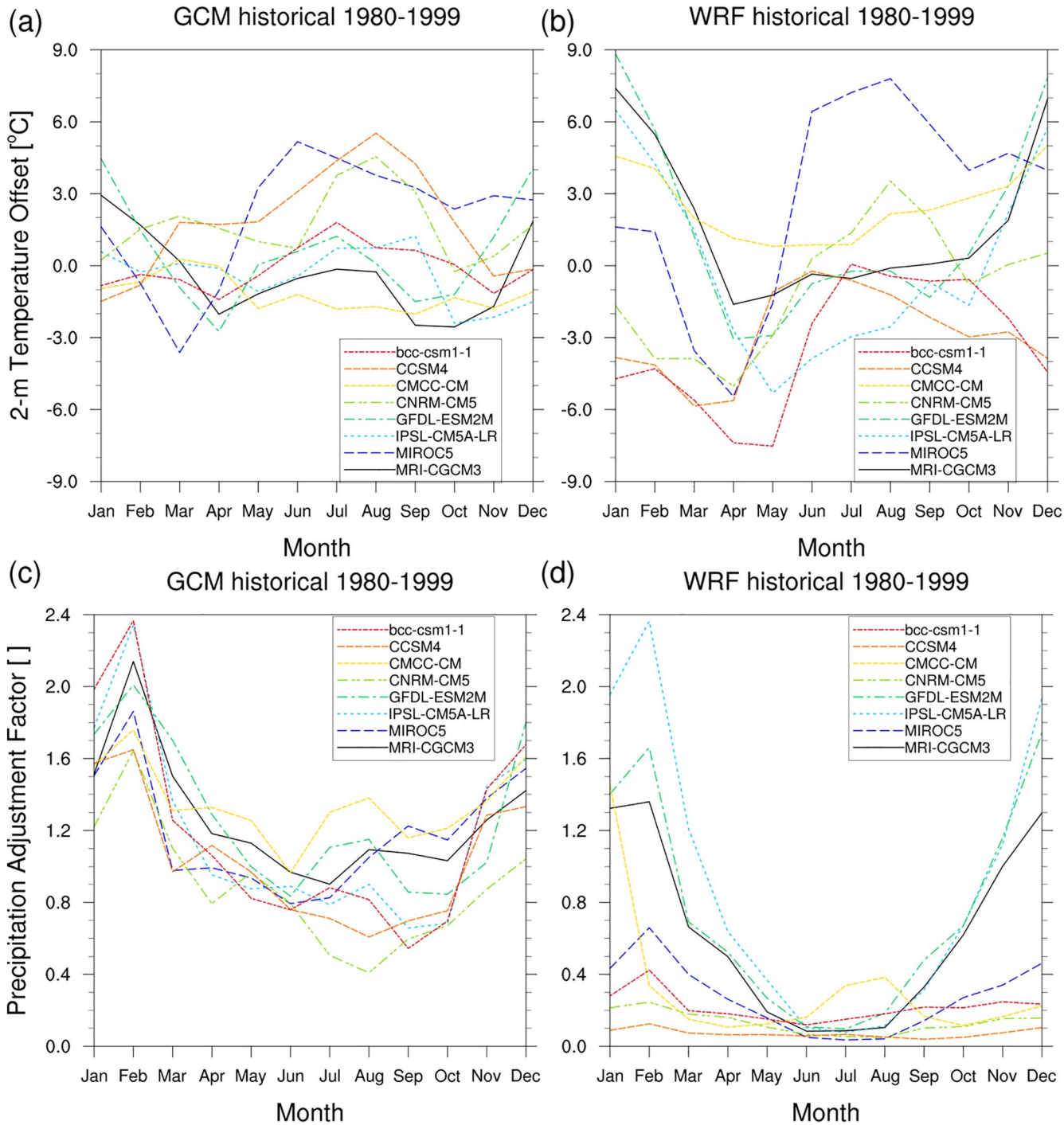

Figure 2. Bias adjustments area-averaged over every grid cell within the state of Minnesota for (a) 2-m temperature difference between GCM runs and PRISM, (b) as (a) but for 2-m temperature difference between WRF runs and PRISM, (c) as (a) but for fraction of PRISM precipitation over GCM runs, and (d) as (b) but for fraction of PRISM precipitation over WRF runs. Please note that the optimum offset in (a) and (b) is 0, whereas the optimum fraction in (c) and (d) is 1.

in Supporting Information S1 provides the bias adjustment factors for snow depth. Their values divert away from 1.0 for smaller absolute snow depth values in spring and fall. We suggest that higher values in WRF snow depth are a direct result of increased precipitation.

MME 2-m temperature increases in each scenario compared to the historical period, particularly in winter (Figure 3). WRF simulates less future warming than the MME when driven by MRI-CGCM3 and GFDL-ESM2M

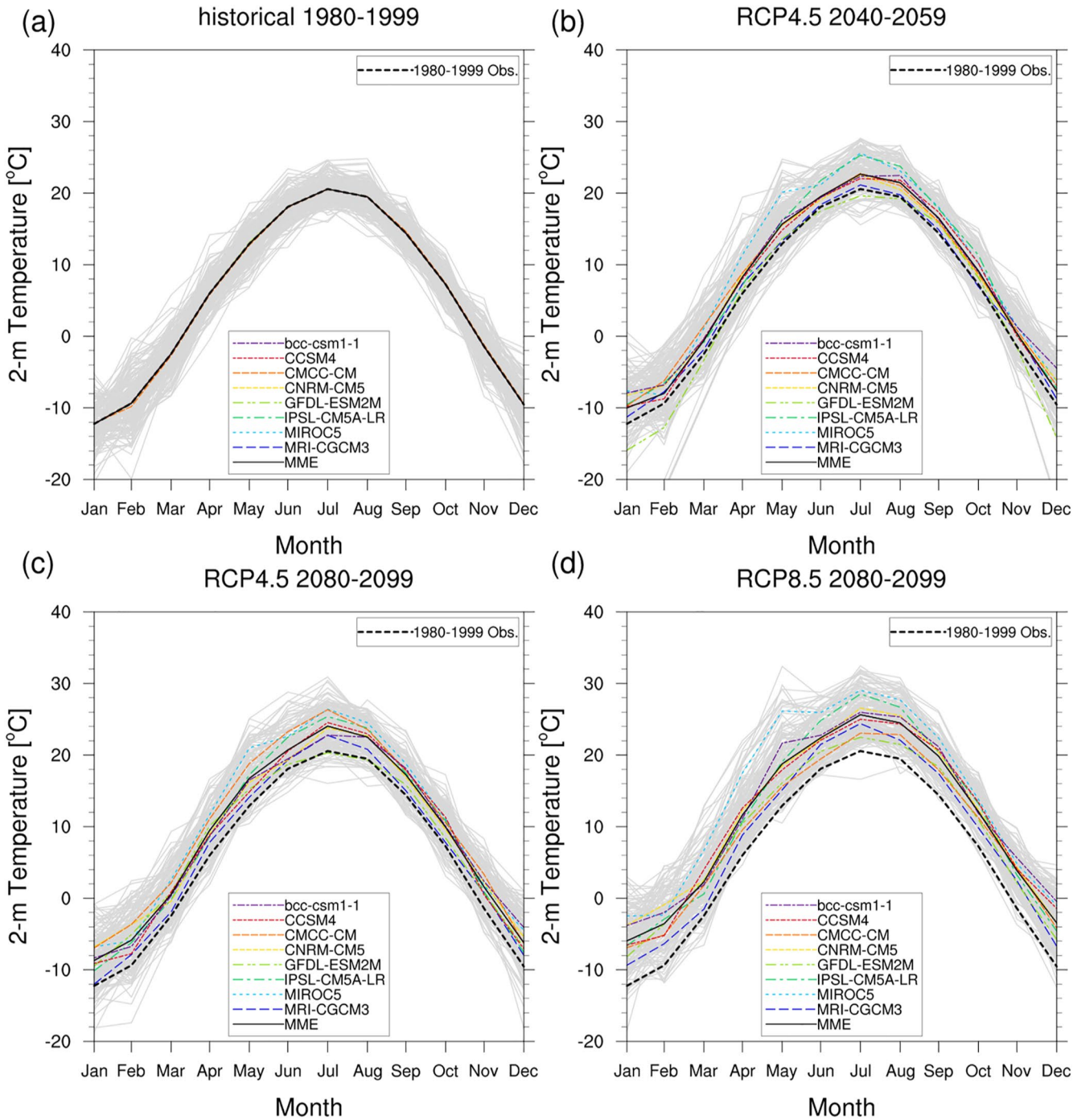

Figure 3. Monthly average 2-meter temperature averaged over every grid cell within the state of Minnesota for each Weather Research and Forecasting (WRF)-downscaled GCM (colors), the multimodel mean (MME; black line), and the PRISM data set (dashed line). Also shown are all years of the 20-year WRF simulations for all GCMS (160 realizations; gray lines).

and generally stronger warming when forced with MIROC5 and IPSL-CM5A-LR. Simulated warming driven by bcc-csm1-1, CCSM4, CMCC-CM, and CNRM-CM5 is relatively close to the MME. Figure S8 in Supporting Information S1 depicts the anomaly time series and overall standard deviation for a more detailed analysis of future trends, which does not only show the projected temperature increase of 2°C by the midcentury but also results in the individual WRF runs. These include strong warming during the month of May of up to 13°C in the

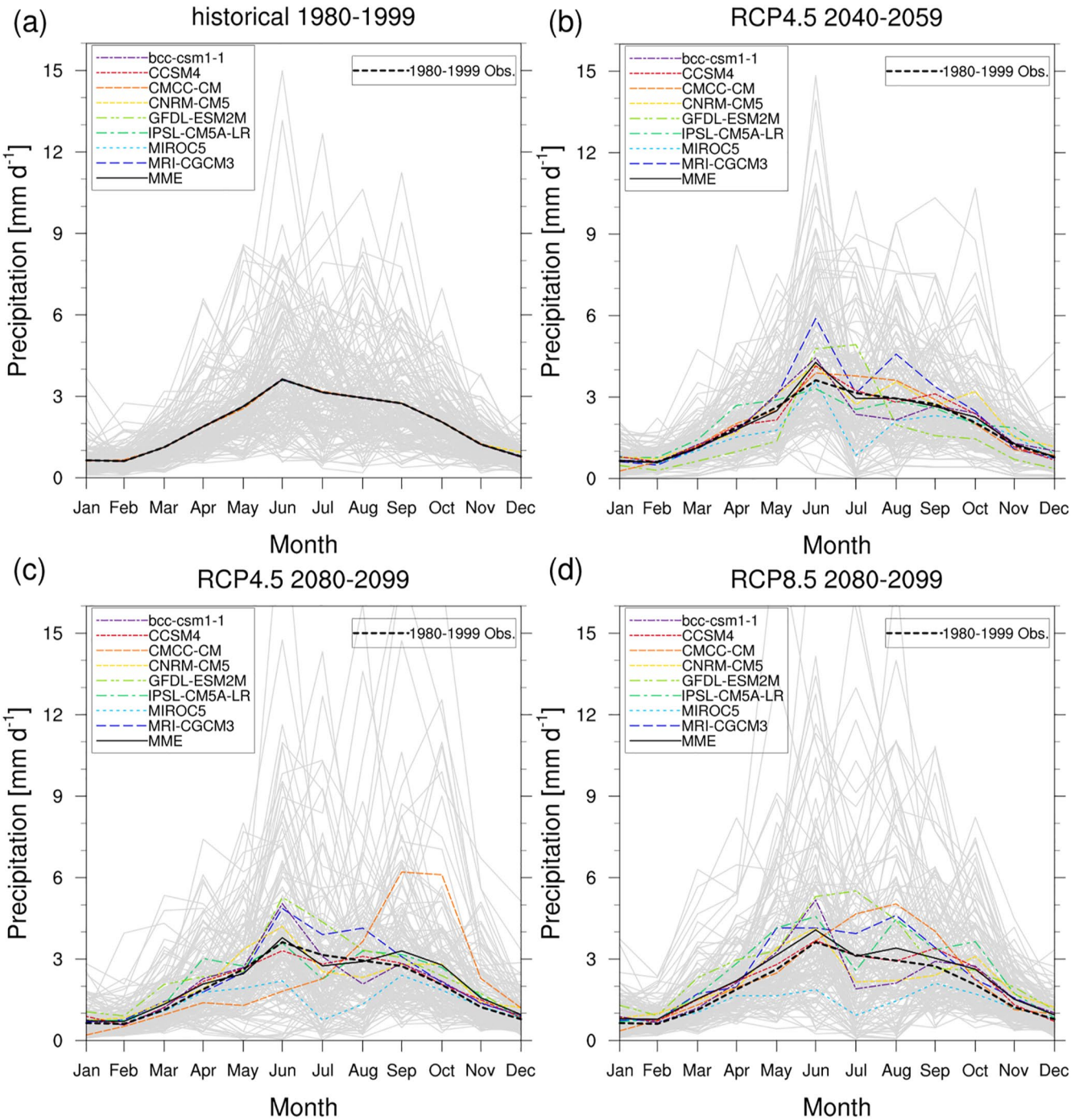

Figure 4. As Figure 3, but for precipitation.

MIROC5-driven runs and an especially weak warming during the month of March of generally less than 1°C in the MRI-CGCM3-driven runs.

Simulated precipitation variability (Figure 4) increases in spring and summer, especially in the late 21st century. Early summer MME rainfall increases in the mid-century and in the RCP8.5 late-century scenarios, while fall MME rainfall increases in both scenarios in the late century. There is a very small increase in winter MME precipitation of about 0.1 mm d^{-1} in all scenarios. When WRF is driven with GFDL-ESM2M and MRI-CGCM3, increases in summer are strongest with values above 2 mm d^{-1}, whereas the MIROC5-driven simulations show

decreases of up to 2 mm d^{-1} from late spring through early fall in all scenarios. WRF-forced simulations of precipitation from CMCC-CM are notably different from those of other models, with large increases of up to 4 mm d^{-1} in the fall for both late 21st-century simulations. As with temperature, precipitation from WRF driven with bcc-csm1-1, CCSM4, and CNRM-CM5 is closest to the MME. Anomaly time series and standard deviation for precipitation and the related snow depth are displayed in Figures S9 and S10 in Supporting Information S1.

3.2. Spatial Distributions

Historical 20-year average winter (Figure 5a) and summer (Figure 6a) MME 2-meter temperatures illustrate the strong north-south temperature gradient in the state. Anomalies of future winter MME projections (Figures 5b–5d) show that temperature increases are strongest along the northern border in the mid-century runs (Figure 5b), throughout much of the northern half of the state in RCP4.5 by the end of the century (Figure 5c) and throughout most of the northern half of the state in the RCP8.5 scenario (Figure 5d).

The increased rate of warming in the north is suggested to be related to both synoptic-scale warming (Wang et al., 2017; their Figure 8) as well as reduced albedo from reduced snow cover, which results in increases in average winter temperature ranging from ∼1°C by the mid-century to 6°C by the end of century in RCP8.5 (Figure 5d). This warming trend can be observed across Minnesota (Runkle et al., 2017; their Figure 1) and our simulations suggest that the trend will continue. Lakes will be ice-free for longer periods and the resulting decrease in albedo will contribute to local winter warming. The average summer temperature shows a more homogeneous increase across the state that ranges from ∼1°C by the mid-century (Figures 6b) to 5°C by the end of the century in the RCP8.5 scenario (Figure 6d). These simulated future increases in average summer temperature contrast with observations of average summer temperature across the state that do not have a significant trend in the historical record (Runkle et al., 2017; their Figure 2a).

Some of the future simulations also do not depict significant temperature changes by the mid-century, especially GFDL-ESM2M and MRI-CGCM3, whereas others show a much stronger warming. Strong mid-century warming of about 4°C occurs with bcc-csm1-1 and CNRM-CM5 forcing in winter and with IPSL-CM5A-LR and MIROC5 forcing in summer (Figures 3b and S8 in Supporting Information S1), which is also depicted in the detailed maps of temperature trends for different GCM input data (Figures S11 and S12 in Supporting Information S1). The stronger warming in the northern parts of the state in the MME is consistent with most model simulations, only CCSM4 and MRI-CGCM3 show a stronger warming in southern and central Minnesota during both seasons and GFDL-ESM2M only during summer. CNRM-CM5 and MIROC5 project a more pronounced negative west-east gradient in winter temperature change than most models, only simulations forced with MRI-CGCM3 and in RCP4.5 also CMCC-CM result in a positive west-east gradient during both seasons. In GFDL-ESM2M, this appears only in winter. Input data from CCSM4, CMCC-CM, and IPSL-CM5A-LR lead to the strongest response over lakes. In summer, increased evaporation over lakes mitigates local warming.

According to the statewide average analysis of precipitation (Figure 4), most of the change in future precipitation occurs in spring and early summer; therefore, we analyze spring average MME precipitation (rain and snow water equivalent) here. Spring average MME precipitation across Minnesota is strongest in the southeast portion of the state and weakest in the northwest (Figure 7a). Simulated precipitation changes by the mid-century differ among WRF runs with some runs showing spring increases (e.g., driven with IPSL-CM5A-LR) and some showing decreases (e.g., driven with MIROC5 and GFDL-ESM2M; Figure 4b), which together result in no significant changes in spring average precipitation across the state (Figure 7b). By the end of the century, spring precipitation is projected to increase slightly in the far north of the state in the RCP4.5 scenario (Figure 7c) and by up to 1 mm d^{-1} in the northern half of the state as well as the southern portion of the domain in Iowa in RCP8.5 (Figure 7d). This is in contrast to statistical projections from Localized Constructed Analogs (LOCA; Pierce et al., 2014), where the strongest precipitation increase occurs in the northeastern and central parts of the state (Figure S13 in Supporting Information S1). This is similar to the historical trend (NCEI, 2021). Our results show that the greatest future increase in rainfall is projected to occur in the northern part of the state indicate a change in regional circulation, and spring average rainfall across the state will become more homogeneous. Winter average MME precipitation is projected to increase slightly, with a statistically significant increase by end of century of up to 0.25 mm d^{-1} in RCP8.5 (not shown).

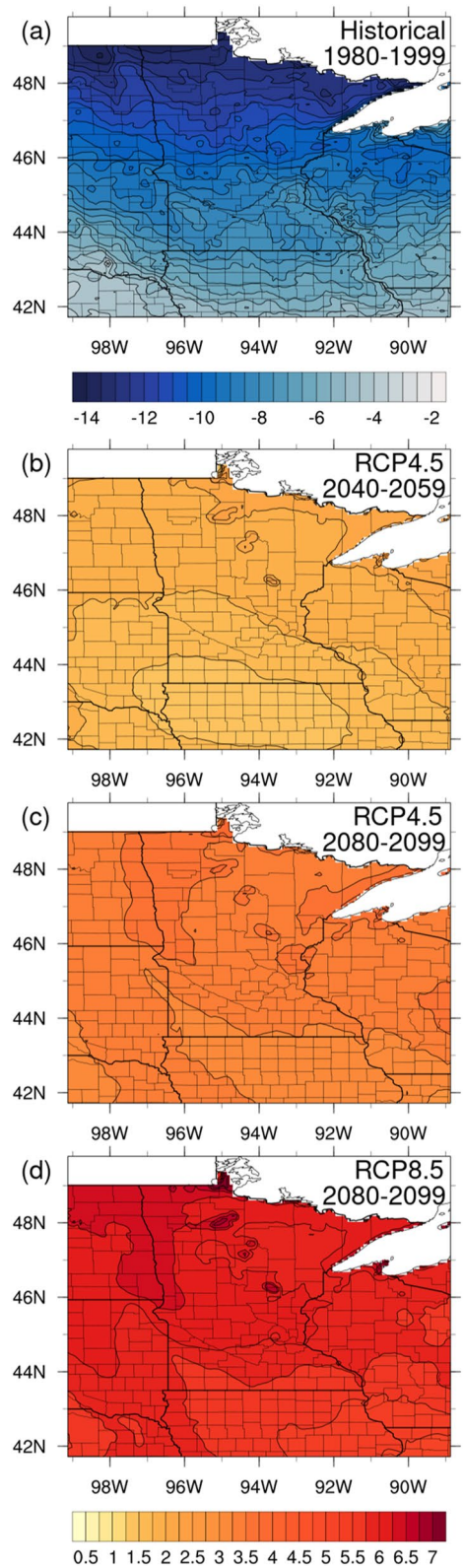

Figure 5. Average winter (December–February) MME 2-meter temperature in °C for (a) historical simulations and (b)–(d) anomalies of each RCP scenario compared to the historical period. Shading in (b)–(d) indicates statistically significant changes over U.S. land points at the 95% confidence interval. Please note that there is a different color bar for (a) than for (b)–(d).

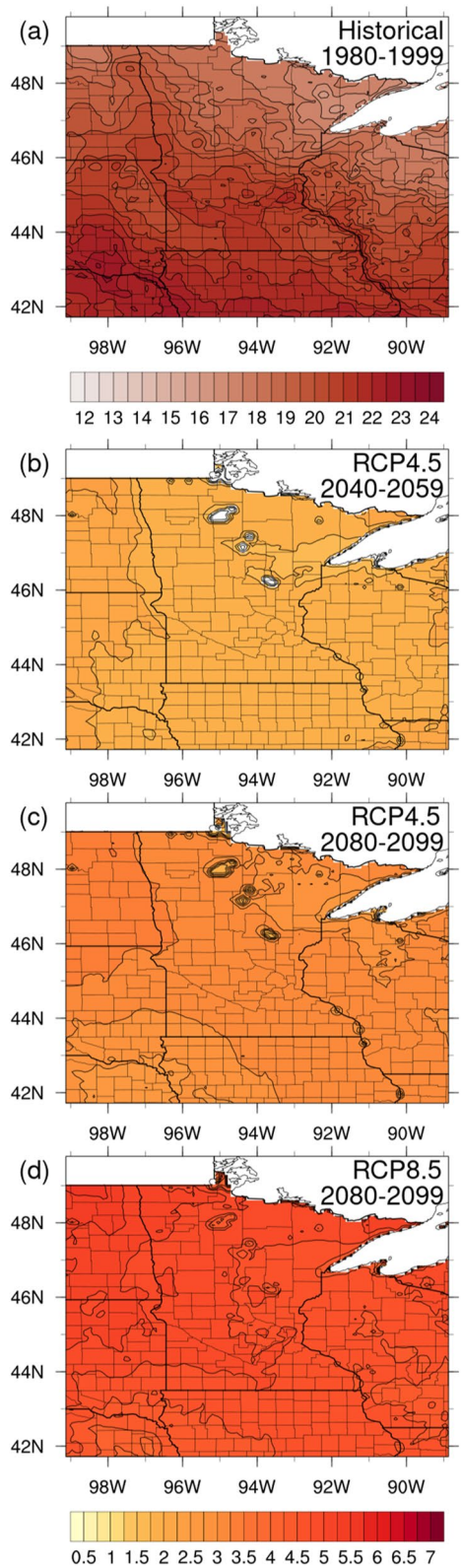

Figure 6. As Figure 5, but for summer (June–August).

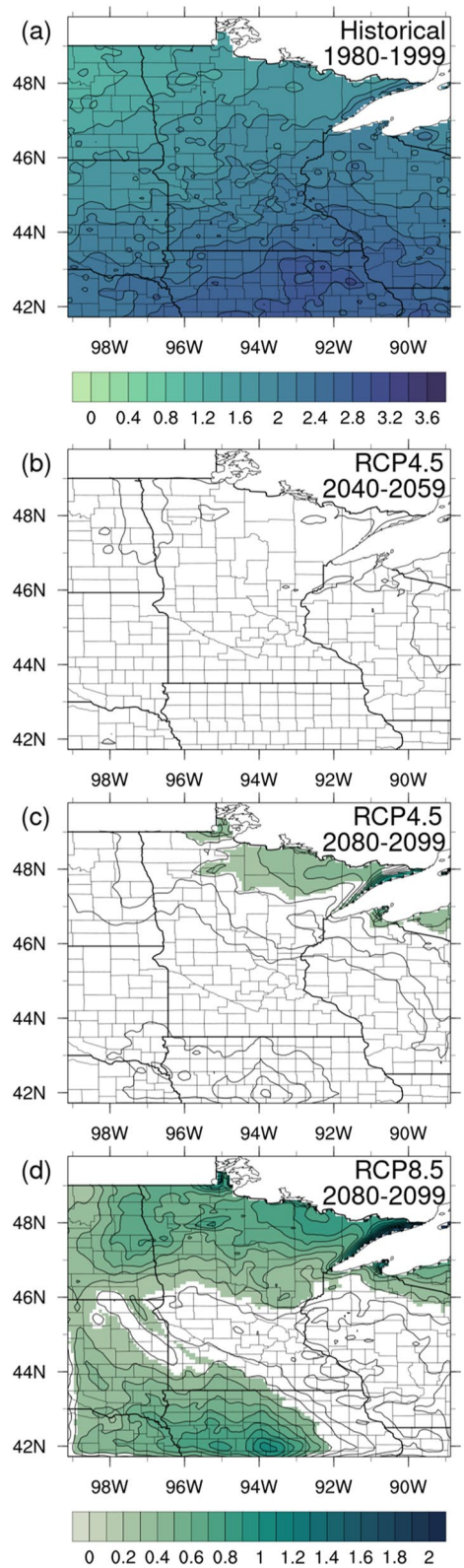

Figure 7. As Figure 5, but for precipitation and precipitation anomalies in mm d^{-1} in spring (March–May).

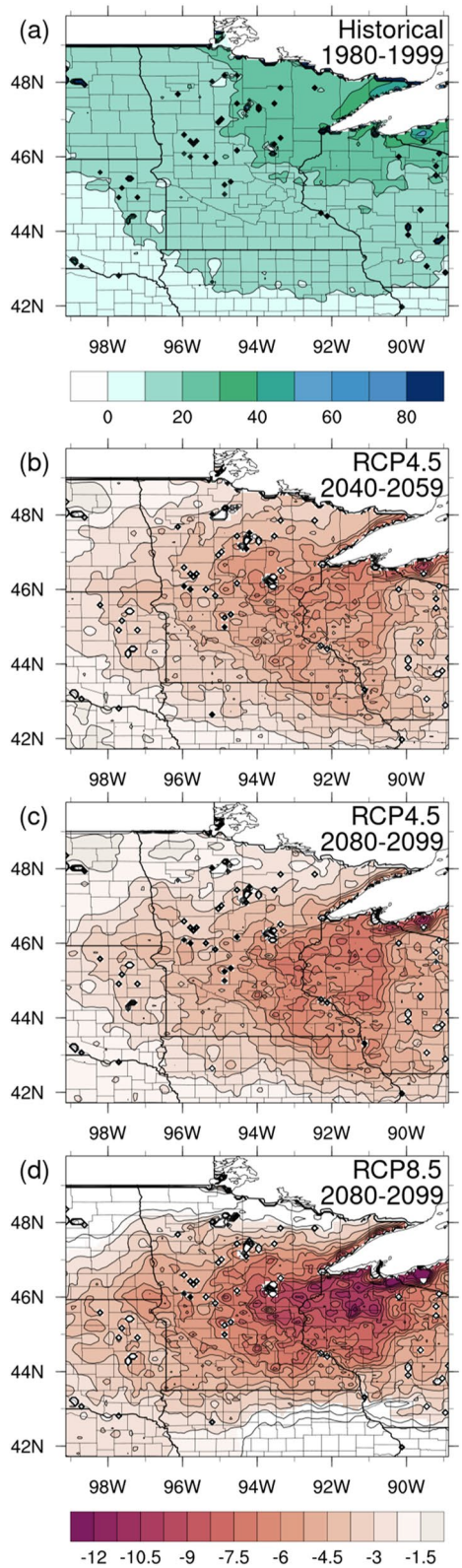

Figure 8. As Figure 5, but for MME snow depth and snow depth anomalies (cm) in winter (December–February).

Average winter MME snow depth generally increases with latitude across the state; however, there is a lobe of lower snow depths stretching northward on the far western side of the state (Figure 8a). Despite the currently observed and projected increases in precipitation, snow depth is projected to decrease across the state except in the northernmost region during the 21st century (Figures 8b–8d) because of increased surface air temperature. Strongest decreases in snow depth are projected to occur in central Minnesota, where average snow depth is expected to decrease by up to 50% by the middle of the 21st century (Figure 8b). By the end of the 21st century under RCP8.5, this change is expected to also cover southern Minnesota and the maximum reduction in snow depth reaches more than 12 cm. While snow depth over the northernmost part of the state remains virtually unchanged, the simulations show significant decreases in snow depth along the Minnesota North Shore and into much of Wisconsin exceeding 12 cm. These regions include part of the U.S. National Forest system and are at risk of decreasing revenues in winter recreation as well as threats to ecosystem health from pests that may survive warmer winters (Govindan & Hutchison, 2020; Venette & Hutchison, 2021).

The average MME number of days per year when snow depth meets or exceeds a threshold of 2.54 cm (equivalent to one inch) follows a similar pattern as average MME snow depth (Figure 9a). Warmer winters result in fewer days with snow cover on the ground. Significant decreases in days per year with snow cover above one inch are found over central and southeast Minnesota and western Wisconsin of up to 40 days per year by the mid-century (Figure 9b). By the end of the century in the RCP8.5 scenario, there are up to 55 fewer days of snow cover in Minnesota and more than 60 fewer days in central Wisconsin (Figure 9d). Because of the large uncertainty of observed snow depth, we also provide non adjusted snow depth values in Figures S14–S16 in Supporting Information S1. They complement Figures S10 in Supporting Information S1 and Figures 8 and 9, and although snow depth is generally lower in observations, the days per year with snow cover are remarkably similar, which suggests that the number of snow events is similar, despite the higher snowfall rate in the WRF simulations.

The goal of this study is to develop a dynamically downscaled climate data set for Minnesota to be used for impact studies. This data set will be useful if it provides value to previously developed, well-tested data sets (i.e., higher resolution while broadly agreeing with other projections). While there are differences in the number of GCMs, time periods, and downscaling methods between our study and that of the National Climate Assessment (NCA), our results are consistent in magnitudes and patterns. For example, our statewide average annual temperature increases (Figures 3b–3d) agree broadly with Midwest average projected increases for RCP4.5 by mid-century (Δ 2.3°C) and for end of century for RCP4.5 (Δ 3.1°C) and RCP8.5 (Δ 5.3°C) in Table 6.4 of the NCA (Vose et al., 2017).

The benefits of downscaling are highlighted for a variable like precipitation that varies strongly in space and time and for which variability is projected to increase in the future. Like our analysis, the NCA found more significant changes in projected precipitation in winter and spring than in fall and summer (Easterling et al., 2017). While their analysis shows a homogeneous increase in winter and spring precipitation for RCP8.5 by the end of the century of about 20%, we found a smaller though statistically significant increase in winter precipitation and more spatial variability in projected spring precipitation. Our projected RCP8.5 end of the century spring precipitation ranges from no statistically significant change in the southern portion of the state to a 12%–30% increase in the central region and a 30%–60% increase in the north. While our analysis provides a more detailed projection of future precipitation than the NCA, we note that there are limitations to our analysis because of the single regional climate model used to downscale data and the single method of bias adjustment we employed (Laux et al., 2021). Future studies will examine alternate methods of bias adjustment of this data set.

The data presented here are immediately useful for impact studies of agricultural, energy, economic, and other ecosystem service sectors of Minnesota and will be a baseline for comparison with future downscaling efforts of CMIP6 (Stouffer et al., 2017). Multimodel ensemble values of temperature and precipitation are available at a variety of user-defined domains from climate.umn.edu (The Minnesota Department of Natural Resources Climate Explorer Tool), and all daily data are available for download at the University of Minnesota Digital Conservancy website. Other raw data are available upon request.

4. Conclusions

The present study describes a high-resolution regional climate modeling effort over the U.S. state of Minnesota that is already providing input for various projects, including improved projections of weather extremes, management of infrastructure, industry, and water resources (Noe et al., 2019) as well as the tracking of invasive species

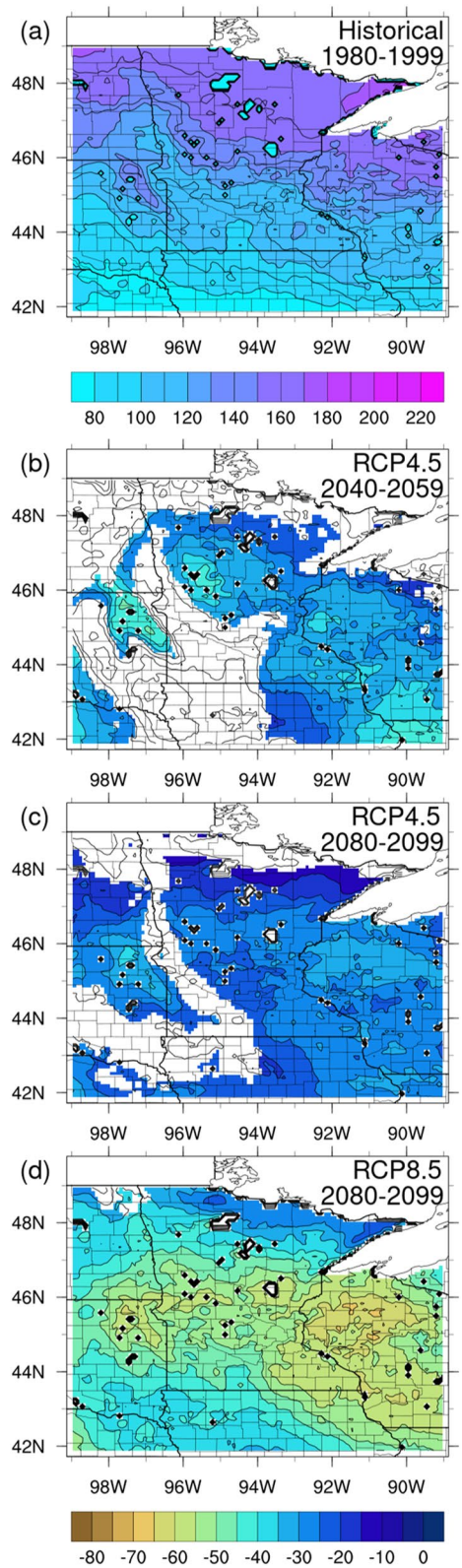

Figure 9. As Figure 5, but for MME days per year and difference in days per year with snow depth above 2.54 cm (one inch).

(Govindan & Hutchison, 2020; Venette & Hutchison, 2021). This state-level downscaling effort links climate projections to decision-making within regional communities. Snow depth simulations emphasize the need for detailed modeling efforts of the hydrological cycle, especially over high-latitude climates.

Data Availability Statement

The daily WRF model data are hosted at the University of Minnesota Digital Conservancy website at: https://doi.org/10.13020/YV29-JY19. CMIP5 forcing data were obtained from the World Data Center for Climate (WDCC) hosted by the German Climate Computing Center (DKRZ) at https://cera-www.dkrz.de/WDCC/ui/cerasearch/q. Monthly temperature and precipitation observations for 1981–2000 were made available by the PRISM group at http://www.prism.oregonstate.edu/recent, and the snow depth analysis was provided by NSIDC at https://doi.org/10.5067/0GGPB220EX6A.

Acknowledgments
The authors acknowledge Keith J. Harding and the Minnesota Supercomputing Institute at the University of Minnesota for providing resources that contributed to the research results reported within this paper (http://www.msi.umn.edu). Funding for this project was provided by a grant from the Legislative-Citizen Commision on Minnesota Resources Grant Number: M. L. 2014, Chp. 312, Sec. 8 to the Minnesota Invasive Terrestrial Plants and Pests Center (http://www.mitppc.umn.edu), and by a grant from the Minnesota Environment and Natural Resources Trust Fund Grant Number: M. L. 2015, Chp. 76, Sec. 2, Subd. 04a (http://www.legacy.mn.gov) as recommended by the Legislative-Citizen Commission on Minnesota Resources. The Trust Fund is a permanent fund constitutionally established by the citizens of Minnesota to assist in the protection, conservation, preservation, and enhancement of the state's air, water, land, fish, wildlife, and other natural resources. Currently, 40% of net Minnesota State Lottery proceeds are dedicated to growing the Trust Fund and ensuring future benefits for Minnesota's environment and natural resources. The authors are grateful to three anonymous reviewers for their insightful comments.

References

Ashfaq, M., Rastogi, D., Mei, R., Kao, S.-C., Gangrade, S., Naz, B. S., & Touma, D. (2016). High-resolution ensemble projections of near-term regional climate over the continental United States. *Journal of Geophysical Research: Atmospheres*, *121*, 9943–9963. https://doi.org/10.1002/2016JD025285

Bekryaev, R. V., Polyakov, I. V., & Alexeev, V. A. (2010). Role of polar amplification in long-term surface air temperature variations and modern Arctic warming. *Journal of Climate*, *23*, 3888–3906. https://doi.org/10.1175/2010JCLI3297.1

Boé, J., Terray, L., Habets, F., & Martin, E. (2007). Statistical and dynamical downscaling of the Seine basin climate for hydro-meteorological studies. *International Journal of Climatology*, *27*, 1643–1655. https://doi.org/10.1002/joc.1602

Broxton, P., Zeng, X., & Dawson, N. (2019). *Daily 4 km gridded SWE and snow depth from assimilated in-situ and modeled data over the conterminous US, version 1*. NASA National Snow and Ice Data Center Distributed Active Archive Center. https://doi.org/10.5067/0GGPB220EX6A

Bruyère, C. L., Done, J. M., Holland, G. J., & Fredrick, S. (2014). Bias corrections of global models for regional climate simulations of high-impact weather. *Climate Dynamics*, *43*, 1847–1856. https://doi.org/10.1007/s00382-013-2011-6

Callendar, G. S. (1938). The artificial production of carbon dioxide and its influence on temperature. *Quarterly Journal of the Royal Meteorological Society*, *64*, 223–240. https://doi.org/10.1002/qj.49706427503

Dai, Y., Zeng, X., Dickinson, R. E., Baker, I., Bonan, G. B., Bosilovich, M. G., et al. (2003). The common land model. *Bulletin of the American Meteorological Society*, *84*, 1013–1023. https://doi.org/10.1175/BAMS-84-8-1013

Daly, C., Slater, M. E., Roberti, J. A., Laseter, S. H., & Swift, L. W. (2017). High-resolution precipitation mapping in a mountainous watershed: Ground truth for evaluating uncertainty in a national precipitation dataset. *International Journal of Climatology*, *37*, 124–137. https://doi.org/10.1002/joc.4986

Dufresne, J.-L., & Bony, S. (2008). An assessment of the primary sources of spread of global warming estimates from coupled atmosphere–ocean models. *Journal of Climate*, *21*, 5135–5144. https://doi.org/10.1175/2008jcli2239.1

Dunne, J. P., John, J. G., Adcroft, A. J., Griffies, S. M., Hallberg, R. W., Shevliakova, E., et al. (2012). GFDL's ESM2 global coupled climate–carbon Earth system models. Part I: Physical formulation and baseline simulation characteristics. *Journal of Climate*, *25*, 6646–6665. https://doi.org/10.1175/JCLI-D-11-00560.1

Easterling, D. R., Kunkel, K. E., & Arnold, J. R. (2017). Ch. 7: Precipitation change in the United States. *Climate Science Special Report: Fourth National Climate Assessment*, I. https://doi.org/10.7930/J0H993CC

Gent, P. R., Danabasoglu, G., Donner, L. J., Holland, M. M., Hunke, E. C., Jayne, S. R., et al. (2011). The community climate system model version 4. *Journal of Climate*, *24*, 4973–4991. https://doi.org/10.1175/2011jcli4083.1

Giorgi, F., & Mearns, L. O. (1991). Approaches to the simulation of regional climate change: A review. *Review of Geophysics*, *29*, 191. https://doi.org/10.1029/90RG02636

Giorgi, F., Mearns, L. O., & Gutowski, W. J. (2015). Regional dynamical downscaling and the CORDEX initiative. *Annual Review of Environment and Resources*, *40*, 467–490. https://doi.org/10.1146/annurev-environ-102014-021217

Govindan, B. N., & Hutchison, W. D. (2020). Influence of temperature on age-stage, two-sex life tables for a Minnesota-acclimated population of the Brown marmorated stink bug (halyomorpha halys). *Insects*, *11*, 108. https://doi.org/10.3390/insects11020

Harding, K. J., & Snyder, P. K. (2014). Examining future changes in the character of Central U.S. warm-season precipitation using dynamical downscaling. *Journal of Geophysical Research: Atmospheres*, *119*(13), 13116–13136. https://doi.org/10.1002/2014JD022575

Harding, K. J., Snyder, P. K., & Liess, S. (2013). Use of dynamical downscaling to improve the simulation of Central U.S. warm season precipitation in CMIP5 models. *Journal of Geophysical Research: Atmospheres*, *118*(12), 12512–522536. https://doi.org/10.1002/2013JD019994

Harding, K. J., Twine, T. E., VanLoocke, A., Bagley, J. E., & Hill, J. (2016). Impacts of second-generation biofuel feedstock production in the central U.S. on the hydrologic cycle and global warming mitigation potential. *Geophysical Research Letters*, *43*(10), 10773–10781. https://doi.org/10.1002/2016GL069981

Harvey, B. J., Shaffrey, L. C., & Woollings, T. J. (2015). Deconstructing the climate change response of the Northern Hemisphere wintertime storm tracks. *Climate Dynamics*, *45*, 2847–2860. https://doi.org/10.1007/S00382-015-2510-8/FIGURES/8

IPCC. (2013) *Climate change 2013: The physical science basis. Contribution of working group I to the fifth assessment report of the intergovernmental panel on climate change*. T. F. Stocker, et al., Eds. (p. 1535). Cambridge University Press.

IPCC. (2021) *Climate change 2021: The physical science basis. Contribution of working group I to the sixth assessment report of the intergovernmental panel on climate change*. In Masson-Delmotte, V., et al. (Eds.), (p. 3949). Cambridge University Press. Retrieved from https://www.ipcc.ch/report/ar6/wg1/

Laux, P., Rötter, R. P., Webber, H., Dieng, D., Rahimi, J., Wei, J., et al. (2021). To bias correct or not to bias correct? An agricultural impact modelers' perspective on regional climate model data. *Agricultural and Forest Meteorology*, *304–305*, 108406. https://doi.org/10.1016/j.agrformet.2021

Liu, C., Ikeda, K., Rasmussen, R., Barlage, M., Newman, A. J., Prein, A. F. (2017). Continental-scale convection-permitting modeling of the current and future climate of North America. *Climate Dynamics*, *491*(49), 71–95. https://doi.org/10.1007/S00382-016-3327-9

Lu, Y., Jin, J., & Kueppers, L. M. (2015). Crop growth and irrigation interact to influence surface fluxes in a regional climate - Cropland model (WRF3. 3—CLM4crop). *Climate Dynamics*, *45*, 3347–3363. https://doi.org/10.1007/s00382-015-2543-z

McGinnis, S., & Mearns, L. (2021). Building a climate service for North America based on the NA-CORDEX data archive. *Climate Services*, *22*, 100233. https://doi.org/10.1016/J.CLISER.2021.100233

Mearns, L. O., Gutowski, W., Jones, R., Leung, R., Mcginnis, S., Nunes, A., & Qian, Y. (2009). *A regional climate change assessment Program for north America*. Eos, Transactions American Geophysical Union, 90, 311. https://doi.org/10.1029/2009EO360002

Mendez, M., Maathuis, B., Hein-Griggs, D., & Alvarado-Gamboa, L.-F. (2020). Performance evaluation of bias correction methods for climate change monthly precipitation projections over Costa Rica. *Water*, *12*, 482. https://doi.org/10.3390/w12020

Molinari, J., & Dudek, M. (1992). Parameterization of convective precipitation in mesoscale numerical models: A critical review. *Monthly Weather Review*, *120*, 3262–3344. https://doi.org/10.1175/15200493(1992)120<0326:pocpim>2.0.co;2

NCEI. (2021). *National trends temperature, precipitation, and drought*. National Centers for Environmental Information (NCEI). Retrieved from https://www.ncdc.noaa.gov/temp-and-precip/us-trends/tavg/win

Noe, R., Keeler, B., Twine, T., Brauman, K., Mayer, T., & Rogers, M. (2019). *Climate change projections for improved management of infrastructure, industry, and water resources in Minnesota*. Retrieved from http://hdl.handle.net/11299/209130

Pierce, D. W., Cayan, D. R., & Thrasher, B. L. (2014). Statistical downscaling using localized constructed Analogs (LOCA). *Journal of Hydrometeorology*, *15*, 2558–2585. https://doi.org/10.1175/JHM-D-14-0082.1

Pincus, R., Batstone, C. P., Hofmann, R. J. P., Taylor, K. E., & Glecker, P. J. (2008). Evaluating the present-day simulation of clouds, precipitation, and radiation in climate models. *Journal of Geophysical Research*, *113*, D14209. https://doi.org/10.1029/2007jd009334

Polyakov, I. V., Alekseev, G. V., Bekryaev, R. V., Bhatt, U., Colony, R. L., Johnson, M. A., et al. (2002). Observationally based assessment of polar amplification of global warming. *Geophysical Research Letters*, *29*, 1878. https://doi.org/10.1029/2001GL011111

Riahi, K., Rao, S., Krey, V., Cho, C., Chirkov, V., Fischer, G., et al. (2011). RCP 8.5—A scenario of comparatively high greenhouse gas emissions. *Climate Change*, *109*, 33–57. https://doi.org/10.1007/s10584-011-0149-y

Runkle, J., Kunkel, K., Frankson, R., Easterling, D., & Champion, S. (2017). *Minnesota state climate summary*. NOAA Technical Report NESDIS 149-MN. 4. pp Retrieved from https://statesummaries.ncics.org/chapter/mn/

Scoccimarro, E., Gualdi, S., Bellucci, A., Sanna, A., Giuseppe Fogli, P., Manzini, E. (2011). Effects of tropical cyclones on ocean heat transport in a high-resolution coupled general circulation model. *Journal of Climate*, *24*, 4368–4384. https://doi.org/10.1175/2011JCLI4104.1

Shi, X., Déry, S. J., Groisman, P. Y., & Lettenmaier, D. P. (2013). Relationships between recent pan-Arctic snow cover and hydroclimate trends. *Journal of Climate*, *26*, 2048–2064. https://doi.org/10.1175/JCLI-D-12-00044.1

Shrestha, M., Acharya, S. C., & Shrestha, P. K. (2017). Bias correction of climate models for hydrological modelling – Are simple methods still useful? *Meteorological Applications*, *24*, 531–539. https://doi.org/10.1002/met.1655

Skamarock, W. C., Klemp, J. B., Dudhia, J., Gill, D. O., Liu, Z., Berner, J., et al. (2008). *A description of the Advanced Research WRF version 3* (p. 125). National Center for Atmospheric Research. http://doi.org/10.5065/D68S4MVH

Stouffer, R. J., Eyring, V., Meehl, G. A., Bony, S., Senior, C., Stevens, B., & Taylor, K. E. (2017). CMIP5 scientific gaps and recommendations for CMIP6. *Bulletin of the American Meteorological Society*, *98*, 95–105. https://doi.org/10.1175/BAMS-D-15-00013.1

Taylor, K. E., Stouffer, R. J., & Meehl, G. A. (2012). An overview of CMIP5 and the experiment design. *Bulletin of the American Meteorological Society*, *93*, 485–498. https://doi.org/10.1175/BAMS-D-11-00094.1

Teutschbein, C., & Seibert, J. (2012). Bias correction of regional climate model simulations for hydrological climate-change impact studies: Review and evaluation of different methods. *Journal of Hydrology*, *456–457*, 12–29. https://doi.org/10.1016/j.jhydrol.2012.05.052

van Vuuren, D. P., Edmonds, J., Kainuma, M., Riahi, K., Thomson, A., Hibbard, K., et al. (2011). The representative concentration pathways: An overview. *Climate Change*, *109*, 5–31. https://doi.org/10.1007/s10584-011-0148-z

Venette, R. C., & Hutchison, W. D. (2021). Invasive insect species: Global challenges, strategies & opportunities. *Frontiers Insect Science*, *1*, 650520. https://doi.org/10.3389/finsc.2021.650520

Voldoire, A., Sanchez-Gomez, E., Salas y Mélia, D., Decharme, B., Cassou, C., Sénési, S., et al. (2012). The CNRM-CM5.1 global climate model: Description and basic evaluation. *Climate Dynamics*, 1–31. https://doi.org/10.1007/s00382-011-1259-y

Vose, R. S., Easterling, D. R., Kunkel, K. E., LeGrande, A. N., & Wehner, M. F. (2017). Chapter 6: Temperature changes in the United States. *Climate Science Special Report: Fourth National Climate Assessment* (Vol.I). https://science2017.globalchange.gov/chapter/6/

Wang, J., Kim, H. M., & Chang, E. K. M. (2017). Changes in northern hemisphere winter storm tracks under the background of Arctic amplification. *Journal of Climate*, *30*, 3705–3724. https://doi.org/10.1175/JCLI-D-16-0650.1

Watanabe, M., Suzuki, T., O'ishi, R., Komuro, Y., Watanabe, S., Emori, S., et al. (2010). Improved climate simulation by MIROC5: Mean states, variability, and climate sensitivity. *Journal of Climate*, *23*, 6312–6335. https://doi.org/10.1175/2010jcli3679.1

Wilks, D. S. (2011). In R. Dmowska, D. Hartmann, & H. T. Rossby (Eds.), *Statistical methods in the atmospheric sciences* (3rd ed., p. 676). Academic Press.

Williams, D. N., Ananthakrishnan, R., Bernholdt, D. E., Bharathi, S., Brown, D., Chen, M., et al. (2009). The earth system grid: Enabling access to multimodel climate simulation data. *Bulletin of the American Meteorological Society*, *90*, 195–205. https://doi.org/10.1175/2008BAMS2459.1

Wu, T., Yu, R., Zhang, F., Wang, Z., Dong, M., Wang, L., et al. (2010). The beijing climate center atmospheric general circulation model: Description and its performance for the present-day climate. *Climate Dynamics*, *34*, 123–147. https://doi.org/10.1007/s00382-008-0487-2

Xu, Z., Han, Y., & Yang, Z. (2018). Dynamical downscaling of regional climate: A review of methods and limitations. *Science China Earth Sciences*, *622*, 62365–62375. https://doi.org/10.1007/S11430-018-9261-5

Yukimoto, S., Adachi, Y., Hosaka, M., Sakami, T., Yoshimura, H., Hirabara, M., et al. (2012). A new global climate model of the meteorological research Institute: MRI-CGCM3—Model description and basic performance—. *Journal of Meteorological Society*, *90A*, 23–64. https://doi.org/10.2151/jmsj.2012-A02

Zeng, X., Broxton, P., & Dawson, N. (2018). Snowpack change from 1982 to 2016 over conterminous United States. *Geophysical Research Letters*, *45*(12), 12940–12947. https://doi.org/10.1029/2018GL079621

Zhang, X., Friedl, M. A., & Schaaf, C. B. (2006). Global vegetation phenology from Moderate Resolution Imaging Spectroradiometer (MODIS): Evaluation of global patterns and comparison with in situ measurements. *Journal of Geophysical Research*, *111*, G04017. https://doi.org/10.1029/2006jg000217

Zhou, W., Leung, L. R., Song, F., & Lu, J. (2021). Future changes in the Great Plains low-level Jet governed by seasonally dependent pattern changes in the north Atlantic subtropical high. *Geophysical Research Letters*, *48*, e2020GL090356. https://doi.org/10.1029/2020GL090356

Zorita, E., & von Storch, H. (1999). The analog method as a simple statistical downscaling technique: Comparison with more complicated methods. *Journal of Climate*, *12*, 2474–2489. https://doi.org/10.1175/15200442(1999)012<2474:tamaas>2.0.co;2